Available online at www.sciencedirect.com
ScienceDirect
C. R. Mecanique 337 (2009) 573–584
COMPTES RENDUS MECANIQUE

Axial development of the mean flow in the entrance region of turbulent pipe and duct flows

Fabien Anselmet [a,*], Fabien Ternat [a,b], Muriel Amielh [a], Olivier Boiron [a], Patrick Boyer [b], Laurence Pietri [a]

[a] *IRPHE, CNRS – Aix Marseille Université – École Centrale Marseille, technopôle de Château-Gombert, 49 rue Joliot-Curie, B.P. 146, 13384 Marseille cedex 13, France*

[b] *IRSN, CE Cadarache, bâtiment 159, 13108 St-Paul Lez Durance, France*

Received 9 June 2009; accepted after revision 10 July 2009

Presented by Paul Clavin

Abstract

The present Note reports a detailed analysis of some of the specific flow properties which are associated with the development region of circular pipes and ducts of square or rectangular cross-sections in turbulent conditions. Indeed, there are no data presently available to determine a priori the acceleration effect which results from the progressive thickening of the boundary layers on the pipe walls. In addition, published results concerning the longitudinal extension of this development region are rather confusing. Through our study, on the one hand, the litigious points are clarified, and, on the other hand, the pertinent grouping of variables (which include the hydraulic diameter D_h and the boundary layer displacement thickness δ_1) providing the parameter relevant for obtaining similarity between all the situations is displayed. ***To cite this article: F. Anselmet et al., C. R. Mecanique 337 (2009).***

Keywords: Turbulence; Pipe flows; Duct flows; Entrance region

1. Introduction

The initial region, also called entrance region, of duct or pipe flows is characterized by specific properties such as a progressive acceleration of the flow which results from the progressive thickening of the boundary layers. This phenomenon is observed whatever the shape of the duct cross-section (circular, square or rectangular). Some experimental data have been published on this phenomenon in the case of turbulent flows, principally by Nikuradse [1], Deissler [2], Melling and Whitelaw [3], Gessner et al. [4] and Demuren and Rodi [5]. These results use the hydraulic diameter D_h to define the dimensionless longitudinal position that gathers well the different results for all the geometries. The hydraulic diameter is defined by $D_h = 4S/P$, where S is the area of the duct cross-section and P is the wetted perimeter. Thus, the normalized centerline velocity U_e/U_b is usually found to be maximum when X/D_h is

* Corresponding author.
E-mail address: fabien.anselmet@irphe.univ-mrs.fr (F. Anselmet).

1631-0721/$ – see front matter
doi:10.1016/j.crme.2009.07.001

Nomenclature

a.r.	aspect ratio of a rectangular section ($= B/d$)
C_f	friction coefficient ($= 2.(u^*/U_e)^2$)
d	height of a rectangular duct or a plane channel
D	diameter of a circular pipe
D_h	hydraulic diameter ($= 4S/P$)
H	shape factor ($= \delta_1/\theta$)
L_e	entrance length
P	wetted perimeter
Re, Re_{D_h}	Reynolds number based on D_h ($= U_b D_h/\nu$)
Re_d	Reynolds number based on d ($= U_b d/\nu$)
Re_x	Reynolds number pertinent for boundary layer development ($= U_e X/\nu$)
S	surface of the cross-section
u^*	friction velocity
U	longitudinal mean velocity
U_e	centerline mean velocity
U_b	bulk velocity

Greek letters

δ	boundary layer thickness
δ_1	boundary layer displacement thickness
θ	boundary layer momentum thickness
ρ	fluid density
ν	fluid kinematic viscosity

comprised between 30 and 40, where U_e denotes the centerline mean velocity for the section at position X and U_b is the bulk velocity. Nonetheless, both the exact position of this maximum and its intensity significantly depend on the global Reynolds number, $\mathrm{Re} = U_b D_h/\nu$. This progressive acceleration has been well known for a long time in wind tunnel design, for which the walls are built slightly diverging downstream in order to annihilate the pressure gradient effect. Usually, a divergent angle value of 0.2 deg is recommended (Jaarsma [6]), but, to the authors' knowledge, no systematic study in turbulent conditions has ever displayed the set of variables that allows collapsing the evolutions of all possible configurations.

On the contrary, in laminar conditions, investigations performed in the 60's–70's (see White [7]) have shown that the variable $(X/D)/(U_b D/\nu)$ provides the collapse of the evolution of U_e/U_b on a unique curve for circular pipes (in this case, D is the pipe diameter), and on another curve for plane channels (i.e. rectangular ducts with very large aspect ratio B/d, where d is the distance between the nearest parallel walls and B the channel width and, in this case, $D = d$).

Consequently, one may wonder whether such a collapse of data can be obtained using a similar dimensionless variable in turbulent conditions, and should provide its physical meaning. Elsewhere, significant discrepancies have been raised in literature concerning the entrance length L_e that characterizes the longitudinal position beyond which full development of the flow is reached (see, for instance, Comolet [8] or White [9]), as some authors recommend the law $L_e/D = 1.6(\mathrm{Re})^{1/4}$ while others suggest $L_e/D = 4.4(\mathrm{Re})^{1/6}$. Indeed, in the usual Reynolds number range (Re between 10^5 and 10^6) where most laboratory studies are performed, the values of L_e/D obtained with these two relations appear to be quite close ($L_e/D \approx 30$–40). A clarification of this critical point is expected. On the one hand, because the use of these formulae at Reynolds numbers larger than 10^6 would lead to significantly different results and, on the other, because those experimental laws do not rely on any solid theoretical development. In particular, the precise criterion to be used for defining L_e is not clear as it is generally not specified in published matter. From our study, we will define a quantitative criterion in Section 3.3 (through relation (2)).

This is why we have undertaken a systematic study in the purpose of changing independently the shape and the size of the section, as well as the bulk velocity, with the aim of finding out which characteristic length should be used (D, d or D_h?). The results we have obtained, which are presented hereafter, reveal that the hydraulic diameter D_h and the boundary layer displacement thickness δ_1 both influence the development region of the flow. From the analysis of these results, an analytical law is proposed and remains valid for circular, square or rectangular (at least for aspect ratios less than 13) sections and allows quantifying precisely the phenomenon.

2. Numerical procedure

The objective of our numerical study is to obtain a wider range of variation of the key parameters, such as the Reynolds number, than is available from published experimental data and to only focus on the purpose of the present

Table 1
Geometries of pipes and ducts used for numerical computations.

	d (m)	D (m)	D_h (m)
Circular pipes		0.16, 0.21, 0.30	0.16, 0.21, 0.30
Ducts ($B = 0.60$ m)	0.32, 0.42, 0.60		0.418, 0.494, 0.60

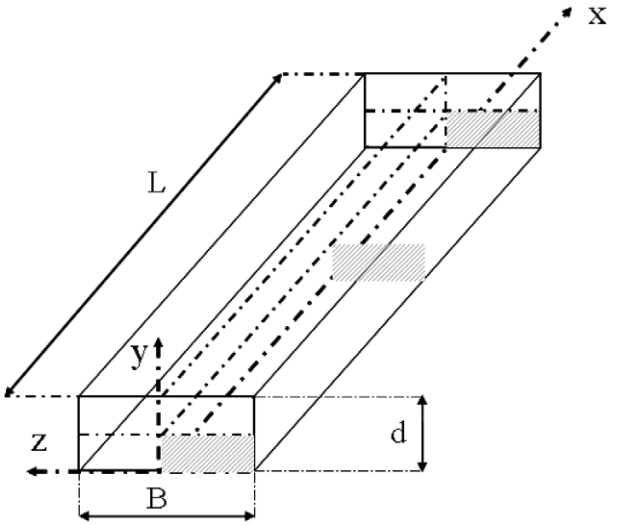

Fig. 1. Scheme of the duct geometry and the associated computation domain (grey quarter of the total volume).

work, which is to study the centerline flow acceleration in the entrance region and to infer the entrance length L_e. It is well known that the k–ε model family is not able to simulate properly non-equilibrium boundary layers. For this reason, the k–ε model could be inappropriate for calculating the flow downstream of the peak in centerline velocity (see e.g. Fig. 2) where secondary flows may become important. However, as this work focused on the development region of the boundary layers, the k–ε approximation proved reasonable since remarkable quantitative agreement with a wide range of experimental data was obtained. The software Fluent (version 6.2) was used. Nevertheless, particular attention had to be devoted to the sizes of the meshes. Ducts with square or rectangular section were modelled for three different configurations (half-height $d/2$ equal to 0.16 m, 0.21 m and 0.30 m and B always equal to 0.6 m, cf. Table 1); the corresponding meshes were designed in three dimensions (only one quarter of the section needed to be represented due to the existence of two symmetry planes, see Fig. 1). Pipes with circular section (diameter D equal to 0.16 m, 0.21 m and 0.30 m) were represented in two dimensions, according to their axisymmetric geometry. The simulated length L then most generally corresponded to 24 m, in order to reach values of the ratio X/D_h at least equal to 50, but a few tests were also performed with $L = 40$ m. Elsewhere, in relation with our practical purposes, the simulated fluid was water whose kinematic viscosity was fixed to $\nu = 10^{-6}$ m^2/s.

The governing equations of the flow model are the three-dimensional, steady, incompressible Reynolds Averaged Navier–Stokes (RANS) equations for the averaged velocity U and pressure P. The closure problem of the RANS is solved using the standard k–ε model (Launder and Spalding [11]). So, accounting for the summation convention (all subscripts range from 1 to 3), the equations of the problem in the computational domain Ω may be given as follows:

$$\rho U_j \frac{\partial U_i}{\partial x_j} = -\frac{\partial P}{\partial x_i} + \frac{\partial}{\partial x_j}\left[(\mu + \mu_t)\left(\frac{\partial U_i}{\partial x_j} + \frac{\partial U_j}{\partial x_i}\right)\right]$$

$$\rho U_j \frac{\partial k}{\partial x_j} = \frac{\partial}{\partial x_j}\left[(\mu + \mu_t/\sigma_k)\frac{\partial k}{\partial x_j}\right] - \rho\overline{u_i' u_j'}\frac{\partial U_i}{\partial x_j} - \rho\varepsilon$$

$$\rho U_j \frac{\partial \varepsilon}{\partial x_j} = \frac{\partial}{\partial x_j}\left[(\mu + \mu_t/\sigma_\varepsilon)\frac{\partial \varepsilon}{\partial x_j}\right] - \rho\overline{u_i' u_j'}\frac{\partial U_i}{\partial x_j}C_{\varepsilon 1}\frac{\varepsilon}{k} - \rho C_{\varepsilon 2}\frac{\varepsilon^2}{k}$$

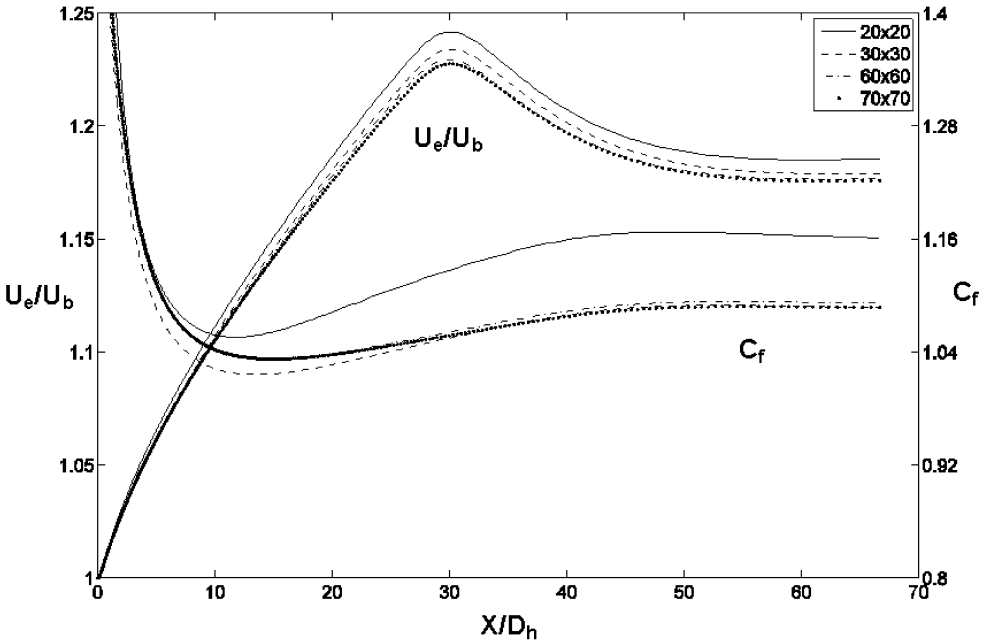

Fig. 2. Comparison of the centerline velocity and friction coefficient (normalized by the friction coefficient value corresponding to the Prandtl law) for several transverse mesh densities. Square duct: $d = D_\mathrm{h} = 0.60$ m $- L = 40$ m $- U_\mathrm{b} = 0.20$ m/s $-$ Re $= 1.2 \times 10^5$.

$$-\rho\overline{u_i' u_j'} + \frac{2}{3}\rho k\delta_{ij} = \mu_\mathrm{t}\left(\frac{\partial U_i}{\partial x_j} + \frac{\partial U_j}{\partial x_i}\right)$$

with: $\mu_\mathrm{t} = \rho C_\mu \frac{k^2}{\varepsilon}$, $C_\mu = 0.09$, $C_{\varepsilon 1} = 1.44$, $C_{\varepsilon 2} = 1.92$, $\sigma_k = 1$ and $\sigma_\varepsilon = 1.3$. U_i is the averaged i velocity component, k the turbulence kinetic energy, ε the dissipation rate, μ, ρ and μ_t respectively the fluid molecular viscosity, the fluid density and the turbulent viscosity of the flow. These field equations must satisfy the following boundary conditions (note that, as explained before, only one quarter of the flow is actually computed for ducts):

Entry section: we set a uniform mean longitudinal velocity distribution such that $U_1 = U_\mathrm{b}$, with $U_2 = U_3 = 0$, associated with a uniform distribution of both the turbulence kinetic energy and the dissipation rate. Values of k and ε are estimated from the classical turbulence intensity, $I = 0.01$, and turbulence length scale, $l = 0.01$ m, by $k = \frac{3}{2}(IU_\mathrm{b})^2$, $\varepsilon = C_\mu^{3/4} k^{3/2}/l$, assuming that for a pipe $l = 0.07 D_\mathrm{h}$ (according to Schlichting [10, p. 568]). Changing l from 0.01 m to 0.02 m or 0.03 m had no influence on the results, so that a unique value of l was used.

Outlet section: we set a uniform pressure $P = 0$ and Neumann homogeneous conditions for k and ε: $\vec{\nabla} k.\vec{n} = \vec{\nabla}\varepsilon.\vec{n} = 0$.

Symmetry conditions are set for the two symmetry planes of the ducts: $\vec{U}.\vec{n} = 0$, $\vec{\nabla}\vec{U}.\vec{n} = \vec{0}$, $\vec{\nabla} k.\vec{n} = \vec{\nabla}\varepsilon.\vec{n} = 0$.

On the walls, i.e. on the bottom and lateral sides, we use the classical wall function approach: near the wall, the solution is given by semi-empirical laws of the standard turbulent boundary layer theory. Depending on the non-dimensional distance, $y^+ = yu^*/\nu$, of the first grid cell from the wall, a logarithmic law ($y^+ > 30$) or a linear law ($y^+ < 5$) is employed for the fluid velocity. If the first cell falls in the buffer-layer zone, a smoothing function is used to insure an asymptotic match of the two preceding laws (Fluent [12]).

For each geometry, five runs have been systematically performed with entry velocities U_b equal to 0.2, 0.3, 0.45, 0.6 and 0.75 m/s. The convergence criterion of the resolution of equations has been set to 10^{-6}, requiring between 1500 and 2500 iterations.

Fig. 2 shows a comparison of the centerline velocities and the bottom wall friction coefficients C_f $(= 2.(u^*/U_\mathrm{e})^2)$ in the symmetry plane ($z = 0$) obtained for the square duct ($B = D_\mathrm{h} = 0.60$ m $- L = 40$ m $- U_\mathrm{b} = 0.20$ m/s) and for several mesh densities. The friction coefficient is normalized by the friction coefficient value ($C_{\mathrm{f\ Prandtl}} = \lambda(U_\mathrm{b}/U_\mathrm{e})^2$) corresponding to a fully developed circular pipe flow according to the Prandtl law (e.g. Schlichting [10]), $\frac{1}{\sqrt{\lambda}} = 2\log(\mathrm{Re}\sqrt{\lambda}) - 0.8$, with $\lambda = 2.(u^*/U_\mathrm{b})^2$. Each grid was built with a constant number of 400 nodes in the

Table 2
Non-dimensional first wall-adjacent cell sizes for different mesh densities and for two different distances from the duct entrance, $X = 1$ m $= 1.667 D_h$ and $X = 10$ m $= 16.67 D_h$.

Grid density	20×20	30×30	60×60	70×70
d^+ (1 m)	64	26	2.5	1.1
d^+ (10 m)	51	21	1.91	0.88

longitudinal direction, but different numbers of nodes were used in the transverse directions. The nodes are stretched with an arithmetic progression (reason 1.08), giving rise to the sizes of the first wall-adjacent cell which are reported in Table 2 in terms of d^+. As shown in Fig. 2, we obtain small discrepancy for the two last meshes tested (60×60 and 70×70). The asymptotic C_f values we obtain for $X/D_h > 55$, when the flow is fully developed, are about 5% larger than the $C_{f\,\mathrm{Prandtl}}$ values. Such results are in good agreement with the fact that the use of the hydraulic diameter is known to only allow C_f values to match $C_{f\,\mathrm{Prandtl}}$ values with a 4–5% error. Therefore, for the square duct (with $D_h = 0.60$ m), we chose finally the $60 \times 60 \times 400$ refinement which gives a grid consisting of 1.44×10^6 elements. These large simulations were performed on a cluster of 4 workstations Dell PowerEdge 1600SC (bi-processor Xeon 2.8 GHz – 1Go RAM) in approximately 6 h.

Simulations for geometries with smaller values of D_h used a smaller mesh ($32 \times 60 \times 160$ grid points) which was validated in a similar way. Only 24 m long flows were simulated in a systematic way since D_h is then smaller (see Table 1). Indeed, trial computations performed for 8 m long flows had revealed that much longer domains had to be used for complete development to be achievable (see Fig. 2).

For circular pipe simulations, whose mesh is two-dimensional because of the axisymmetric geometry, the longitudinal distribution of nodes was similar to that described for ducts (with 350 nodes). Vertically 60 nodes were used, with a progression factor equal to 1.035 and the first mesh located at 0.39 mm from the wall (for $D = 0.16$ m, the mesh for $D = 0.21$ m being stretched as for the ducts), resulting in 21 000 quadrilateral cells. For $D = 0.30$ m, 80 mesh nodes were used, with the first mesh located at 0.445 mm from the wall, which results in 28 000 quadrilateral cells.

3. Results

3.1. Mean velocity profiles and associated quantities

Fig. 3 reports the typical velocity distributions obtained in the symmetry plane of the flow ($z = 0$) for the duct with $d = 0.60$ m, in the form of U/U_e vs. y/δ, for all five velocities U_b. As Reynolds numbers Re_x ($= U_e X/\nu$) are larger than 10^6, this figure shows that the dimensionless velocities U/U_e follow the usual power-law evolution, $U/U_e = (y/\delta)^{1/n}$, with $1/n$ about $1/7$, for all five values of the bulk velocity U_b (a detailed discussion of the similarity properties for turbulent pipes and boundary layers is available in Schlichting [10, chap. XXI]). The usually reported slight variation of $1/n$ when Re_x increases can be noted. Very similar results (not shown here) are obtained for the other values of d and for the circular pipes. Data reported in Fig. 3 are related to the station located at $X = 8$ m $= 13.3 D_h$; this station is typical of what is obtained in the development region where the centerline velocity increases quite strongly for increasing X, as a result of the progressive thickening of the wall boundary layers. When the velocity distributions are plotted in terms of U^+ ($= U/u^*$) vs. y^+ (results not shown here), very good agreement with the usual logarithmic distribution is obtained for y^+ larger than about 25. Even though such plots could have been used to evaluate systematically the values of u^* and C_f presented hereafter, we preferred to compute them from the values of the wall stress τ_w provided by Fluent, because this was both more precise and more convenient.

The associated longitudinal evolution of the displacement thickness δ_1 is plotted in Fig. 4, in terms of δ_1/X vs. the Reynolds number Re_x. This evolution is compared with the standard $\mathrm{Re}_x^{-1/5}$ law corresponding to $1/n = 1/7$. When the flow is fully developed and δ_1 has reached an asymptotic constant value, the asymptotic regime is achieved. Since the boundary layer thickness δ is then equal to $d/2$, δ_1 is equal to $d/16$, corresponding to a -1 slope for the reported evolution of δ_1/X.

In Fig. 5, the influence of the pressure gradient is analysed through the longitudinal evolution of the friction coefficient C_f,

$$C_f = 2\frac{\mathrm{d}\theta}{\mathrm{d}x} - \theta\frac{H+2}{\rho U_e^2}\frac{\mathrm{d}P}{\mathrm{d}x}$$

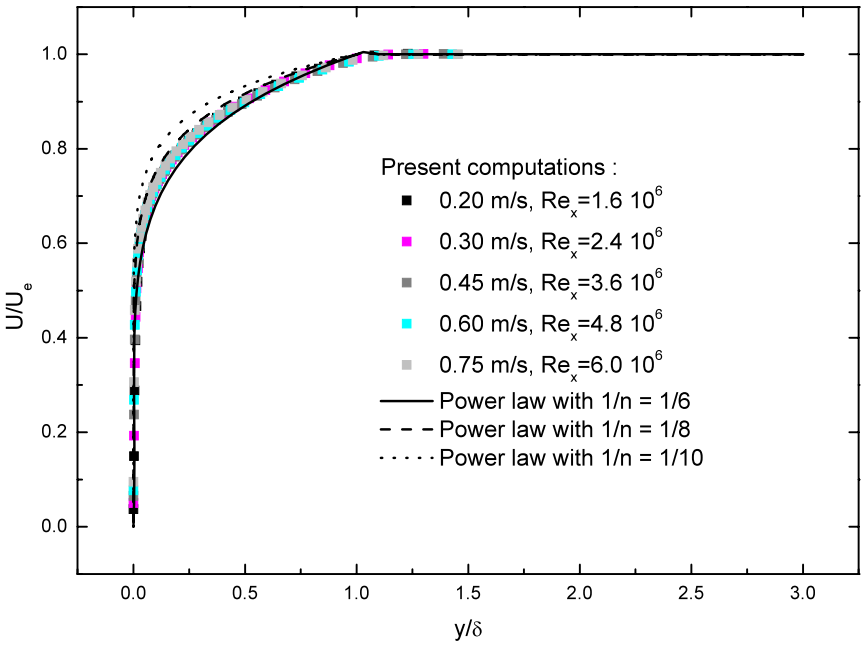

Fig. 3. Mean velocity distributions (in terms of U/U_e and y/δ) obtained at $X = 8\ \text{m} = 13.3D_h$ for the square duct with $d = D_h = 0.60$ m.

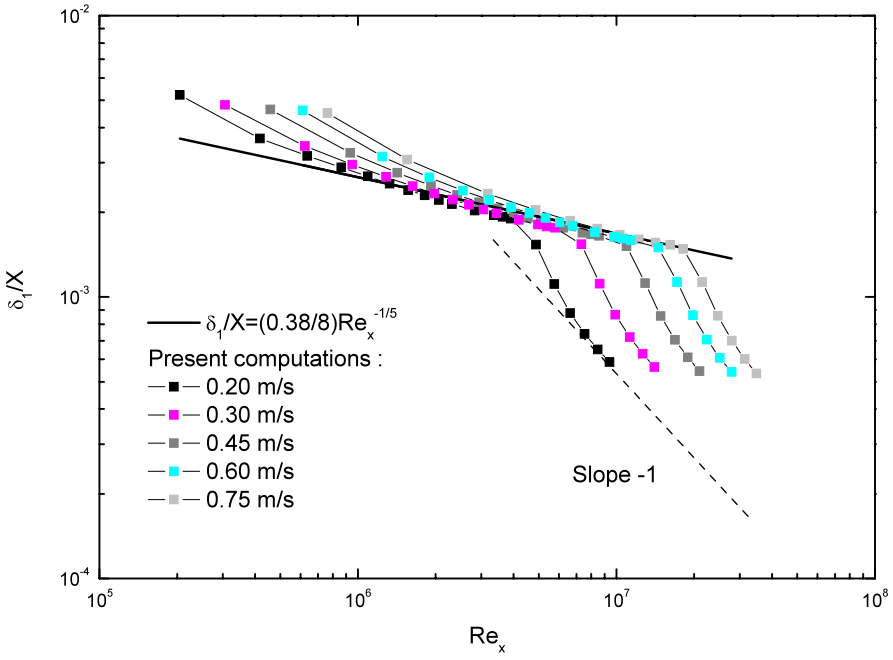

Fig. 4. Longitudinal evolutions of the displacement thickness for the square duct with $d = D_h = 0.60$ m.

(where θ denotes the boundary layer momentum thickness and H the shape factor, $H = \delta_1/\theta$, whose value is about 1.3, value calculated from the relations $\delta_1 = \delta/(n+1)$ and $\theta = \delta n/[(n+1)(n+2)]$, with $1/n = 1/7$). The second term of the right part of the equation which governs the evolution of C_f may be neglected as long as the boundary

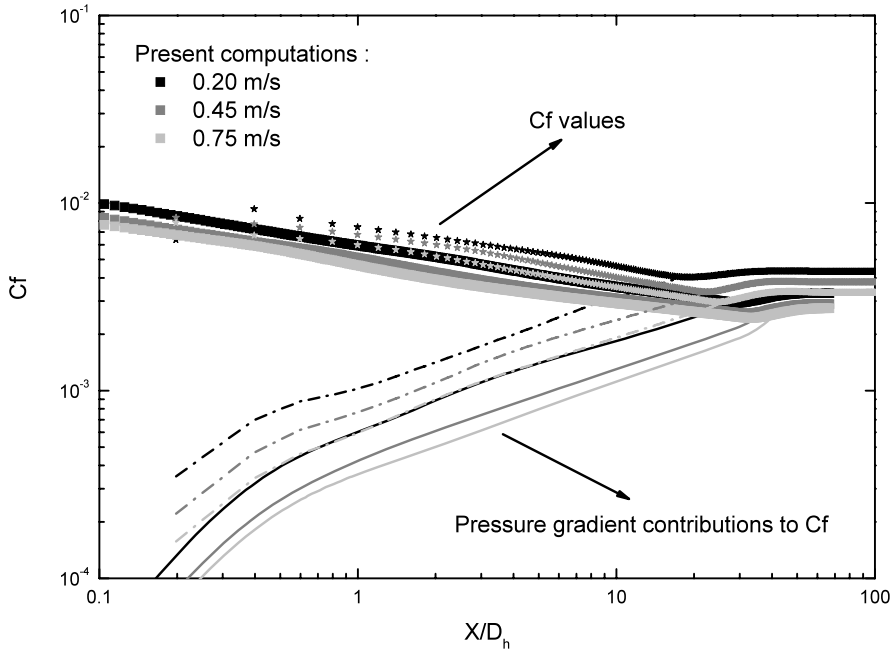

Fig. 5. Longitudinal evolutions of the friction coefficient for the square duct with $d = D_h = 0.60$ m (■, C_f values; —, pressure gradient contributions to C_f) and the circular pipe with $D = D_h = 0.16$ m (★, C_f values; – · –, pressure gradient contributions to C_f).

layer momentum thickness makes it small enough compared to the first term (in practice, this concerns a large part of the flow, i.e. $X < 18$–20 m). Thus, in the entrance region, variations of δ and δ_1 should satisfy the conventional laws,

$$\delta/X = 0.38\mathrm{Re}_x^{-1/5} \quad \text{and} \quad \delta_1 = \delta/8 \tag{1}$$

obtained without pressure gradient with $1/n = 1/7$, as these variations and that of C_f both depend on Re_x. On the contrary, once the flow has reached its fully developed regime, the $\mathrm{d}\theta/\mathrm{d}x$ contribution vanishes and, as expected, the C_f evolution is then only associated to the (constant) pressure gradient. C_f values, as well as δ and δ_1, then remain constant.

3.2. Centerline velocity

Fig. 6 presents the centerline velocity U_e/U_b as a function of the dimensionless distance X/D_h for the different ducts. These results are compared to published data found in the literature (cf. Table 3 for details). Those from Comte-Bellot [13] and Dean [14], that are expressed in terms of X/d in the original paper by Gessner et al. [4], reveal a priori a very different behaviour of these flows with a large aspect ratio (equal or larger than 12 for both studies). But, when they are expressed as a function of X/D_h, they gather well with the other results. Moreover, the observed trend varies sensitively with the global Reynolds number Re but does not seem to depend on the shape of the duct (circular, square or rectangular). The latter only looks to affect the longitudinal position where the centerline velocity U_e/U_b reaches its maximum value. Indeed, for rectangular ducts, the development of the flow is limited by the smallest dimension of the cross-section (i.e. d), for which the corresponding boundary layers first merge on the centerline. For both experiments with an aspect ratio (a.r.) equal or larger than 12, the approximation $D_h = 2d/(1 + 1/(\text{a.r.})) \approx 2d(1 - 1/(\text{a.r.})) \approx 2d$ can be used (valid for B/d larger than 10). In the cases where $D_h \approx 2d$, the maximum values of U_e/U_b are observed at $X/D_h \approx 20$, whereas they are rather at $X/D_h \approx 30$ for the other situations.

In order to highlight the influence of the bulk velocity on the longitudinal velocity U_e/U_b evolution, plots (not shown here) of the same data as for Fig. 6, but with the abscissa changed from X/D_h to U_bX/ν, indicate that the position where U_e/U_b reaches its maximum value is strongly affected. As global variables (C_f, length scales δ/X, δ_1/X and θ/X) are functions of $\mathrm{Re}_x^{-1/5}$, it is therefore logical to represent the centerline velocity results in terms of $(X/D_h).(U_bX/\nu)^{-1/5}$. This is done in Fig. 7, which shows a noticeable collapse of all data on a single line of slope

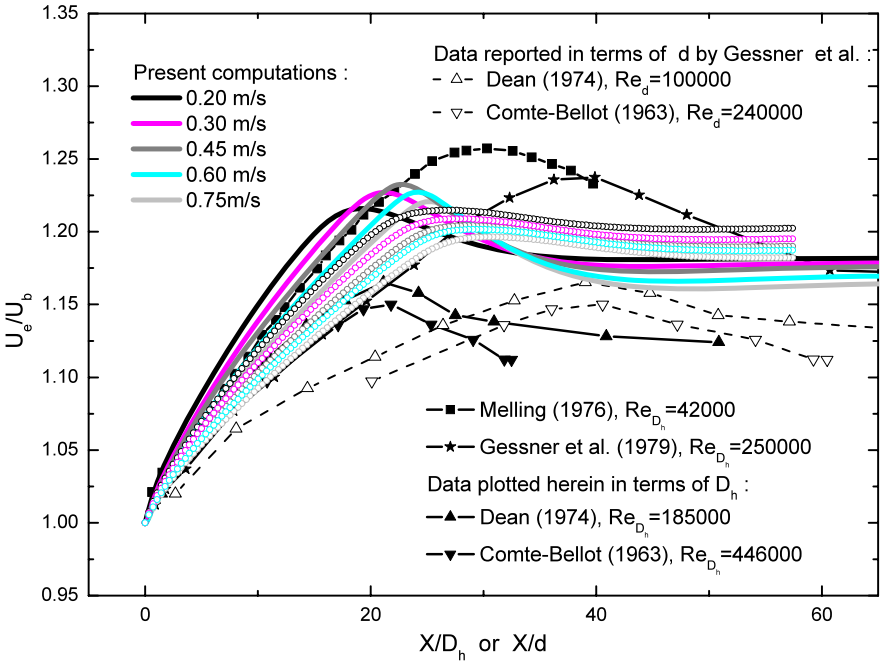

Fig. 6. Longitudinal evolution of the centerline velocity U_e/U_b, in terms of X/D_h. Present computations: —, circular pipe, $D = D_h = 0.16$ m, $32\,000 < \mathrm{Re}_{D_h} < 120\,000$; ∘∘∘, rectangular duct, $d = 0.32$ m, $D_h \approx 0.42$ m, $84\,000 < \mathrm{Re}_{D_h} < 315\,000$.

Table 3
Main characteristics of published experimental data.

	Type of flow	Aspect ratio	D_h (m)	Re_{D_h}
Comte-Bellot [13]	Plane channel	13.3	0.34	446 000
Dean [14]	Plane channel	12	0.09	185 000
Melling and Whitelaw [3]	Square duct	1	0.04	42 000
Gessner et al. [4]	Square duct	1	0.254	250 000

0.185, independently from the type of section and the bulk velocity. From this statement, the same data have been plotted (Fig. 8) in function of δ_1/D_h, because δ_1 quantifies the loss of mass flux in the near-wall region due to the boundary layer: $\delta_1 U_e = \int_0^\infty (U_e - U)\,\mathrm{d}y$. The same grouping as that of Fig. 7 is observed, but the slope of the line is then very close to 4. Even though the collapses provided by the groupings $(X/D_h).(U_b X/\nu)^{-1/5}$ and δ_1/D_h used respectively in Figs. 7 and 8 are not strictly equivalent, the former one being more accurate than the latter one, it has been found interesting to also plot data in terms of δ_1/D_h since this provides a simple physical interpretation whatever the section shape. For circular sections (for which D_h is the pipe diameter D), the mass flux conservation between the entrance section and another one leads to the relation:

$$U_b \frac{\pi}{4} D_h^2 = U_e \frac{\pi}{4} (D_h - 2\delta_1)^2$$

or

$$\frac{U_e}{U_b} = \frac{1}{(1 - 2\delta_1/D_h)^2} \approx 1 + 4\delta_1/D_h$$

when δ_1/D_h is small enough with respect to 1, which is the case here. For a square section duct (D_h is then equal to the length of the square edge), the interpretation is even more direct because there are 4 edges in a square, and then 4 boundary layers are simultaneously developing.

For a rectangular section duct with large aspect ratio, only two boundary layers (those of closest walls separated by the distance d) influence the development of the flow. In this case, the evolution rate is given by $2.\delta_1/d$. But, as D_h is approximately equal to $2d$, this rate is also equal to $4.\delta_1/D_h$.

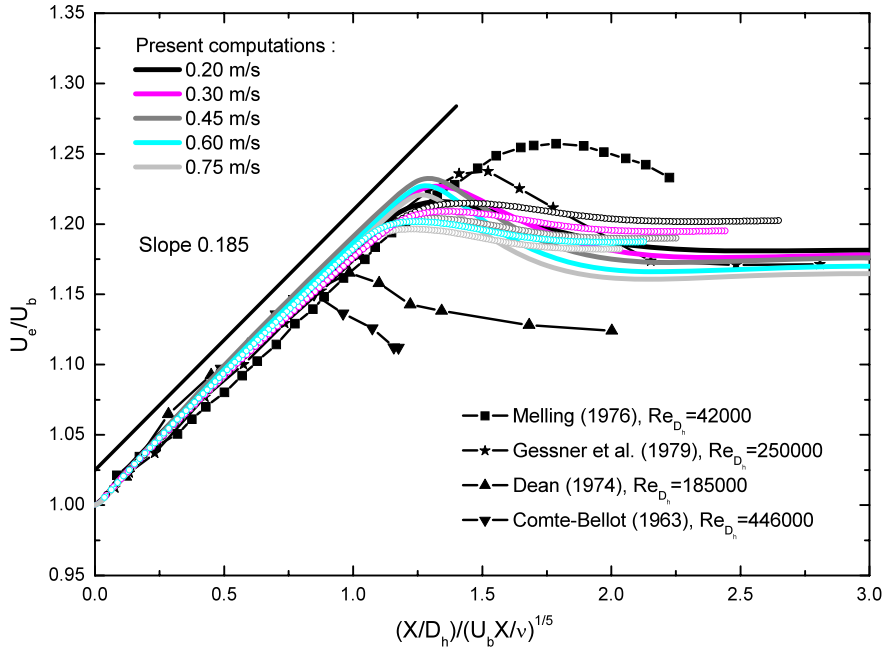

Fig. 7. Longitudinal evolution of the centerline velocity U_e/U_b, in terms of $(X/D_h)/(U_bX/\nu)^{1/5}$.

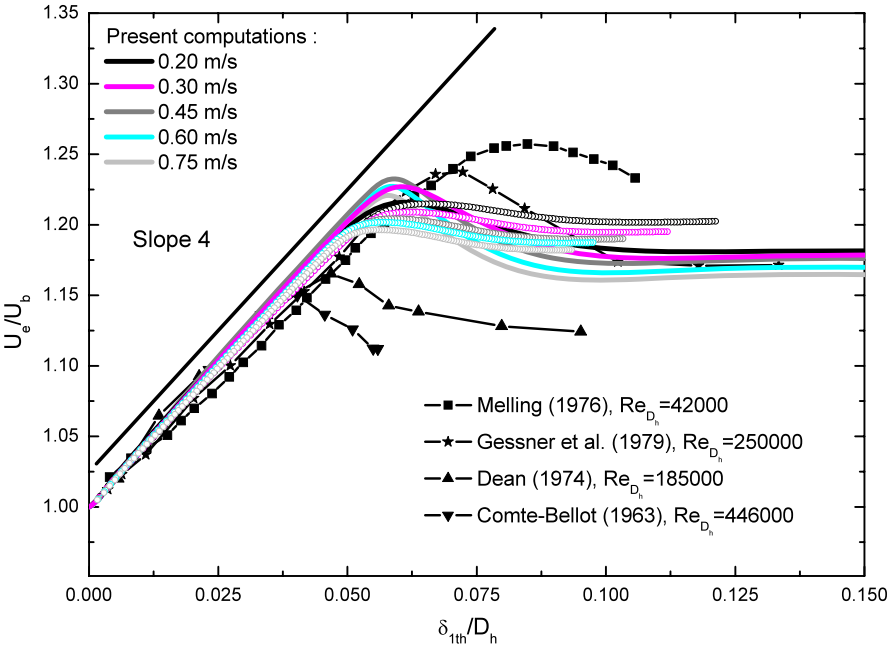

Fig. 8. Longitudinal evolution of the centerline velocity U_e/U_b, in terms of δ_{1th}/D_h. Note that δ_{1th} refers to the δ_1 values inferred from relation (1).

Nonetheless, this result is not as trivial as suggested by the previously developed argumentation. Indeed, in square and rectangular ducts with small aspect ratio, transverse distributions of mean velocities present important three-dimensional effects, which result from the presence of longitudinal eddies in the corners. Therefore, it is not straightforward to find that a combination of only the velocity in the symmetry plane and the thickness δ_1 provides such a simple global characterization of the progressive thickening of the boundary layers. But, independently from

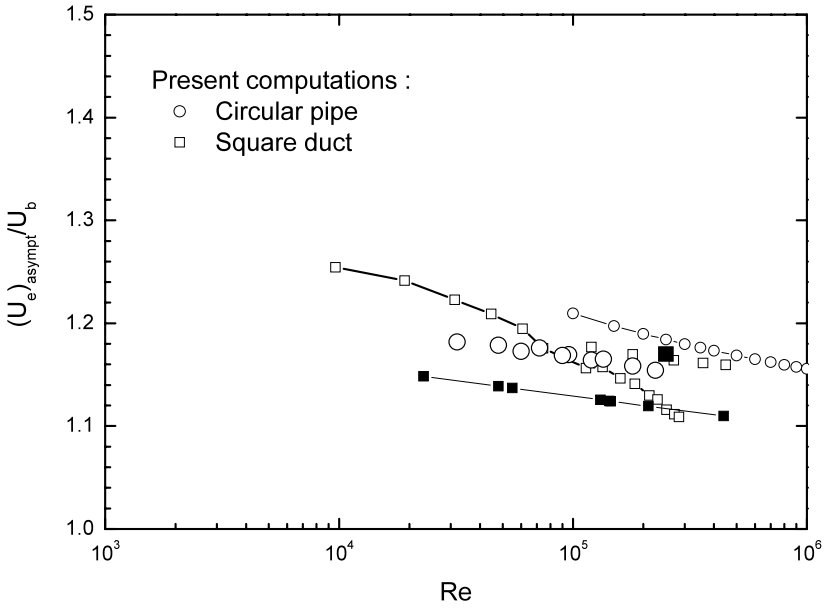

Fig. 9. Asymptotic values of the centerline velocity $(U_e)_{asympt}/U_b$, attained when the flows are fully developed. –○–, compilation of circular pipe experimental data reported by Coantic [15]; –□–, compilation of square duct experimental data reported by Demuren and Rodi [5]; ■, experimental value for the square duct configuration studied by Gessner et al. [4]; –■–, compilation of plane channel experimental data reported by Dean [16].

our simulation choices (RANS modelling), the collapse presented in Fig. 8 for all experimental data (including square ducts and rectangular ducts with a large aspect ratio) in the development region suggests that those secondary flows do not significantly impact on the velocity variation on the centerline of the flow. However, the presented numerical results obtained with the k–ε model, that cannot reproduce such secondary effects and these eddies, provide good agreement with experimental data. Another illustration of the validity of the present results is provided by the evolutions of the asymptotic values of the centerline velocity $(U_e)_{asympt}/U_b$, attained when the flows are fully developed, which are plotted in Fig. 9 as a function of the Reynolds number Re. Our numerical results are fairly consistent with the experimentally determined evolutions, in spite of non-negligible overall scatter. Part of this scatter may result from other quantities (such as the initial turbulence level or integral scale) or features (such as the design of the inlet section) which are generally poorly documented by the authors. It is obviously behind the scope of the present work to first review literature data in this direction and then study the specific influence of these parameters.

3.3. Entrance length

Finally, on the basis of results of Fig. 7, it is possible to infer the entrance length L_e, which corresponds to the longitudinal position where full development of the flow is reached. As stated in the introduction, the latter has been related to the global Reynolds number through two different formulae, commonly used in the literature: $L_e/D = 1.6(\mathrm{Re})^{1/4}$ and $L_e/D = 4.4(\mathrm{Re})^{1/6}$. According to Fig. 7, the full development position can be located between $(X/D_h)/(U_bX/\nu)^{1/5} = 1.25$ and $(X/D_h)/(U_bX/\nu)^{1/5} = 1.75$. More generally, if C denotes the value of the parameter $(X/D_h)/(U_bX/\nu)^{1/5}$ at $X = L_e$, then $(L_e/D_h) = C.(U_bL_e/\nu)^{1/5}$, so that

$$L_e/D_h = C^{5/4}.(U_bD_h/\nu)^{1/4} \tag{2}$$

For $C = 1.25$, we get $L_e/D_h = 1.3(U_bD_h/\nu)^{1/4}$ whereas $C = 1.75$ leads to $L_e/D_h = 2.0(U_bD_h/\nu)^{1/4}$. By this way, we prove that L_e/D_h *must* vary as the power 1/4 of the global Reynolds number Re. As shown in Fig. 10, the two values deduced from the results of Fig. 7 through relation (2) are almost symmetrically located with respect to the value of the pre-factor of the published empirical relation in power 1/4. These values do not validate the published relation in power 1/6, even though, in the considered Reynolds number range (10^5–10^6), numerical values of L_e/D_h remain quite close to these empirical laws. This easily explains why the relation in power 1/6 has been famous so

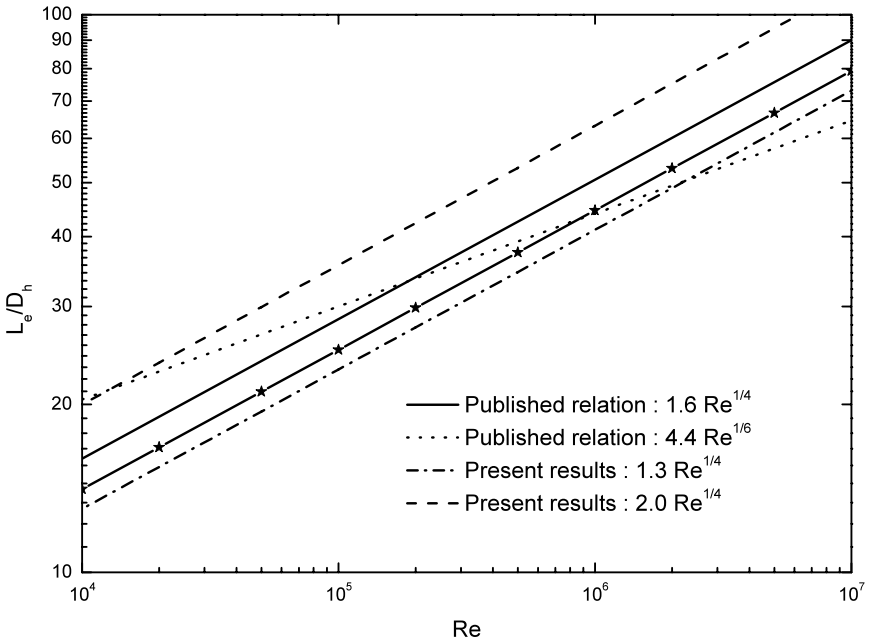

Fig. 10. Entrance length L_e inferred from the centerline velocity data using relation (2): $C = 1.25 - L_e/D_h = 1.3(U_b D_h/\nu)^{1/4}$; $C = 1.75 - L_e/D_h = 2.0(U_b D_h/\nu)^{1/4}$. –★–, adjustment of circular pipe data published by Szablewski [17].

far. Note that the adjustment of circular pipe data published by Szablewski [17] also follows an evolution in power $1/4$ even though this trend was not explicitly displayed in this paper. These results show that L_e/D_h values are in the range 20–30 (for the Re values considered herein): these values correspond to the longitudinal positions where U_e/U_b maxima are reached rather than where U_e/U_b reach their asymptotic constant values. They also correspond to the positions where C_f evolutions (see Fig. 5) switch from the $(\mathrm{Re}_x)^{-1/5}$ regime to the asymptotic regime where C_f values are constant. Similarly, when the δ_1/X evolutions, which are reported in Fig. 4 in terms of Re_x, are plotted as a function of the quantity $(X/D_h).(U_b X/\nu)^{-1/5}$, the switch of regime is obtained for $(X/D_h).(U_b X/\nu)^{-1/5}$ about 1.4, which is remarkably consistent with the U_e/U_b and C_f evolutions. We therefore argue that, even though the definition of the entrance length given by relation (2) does not correspond to the position where U_e/U_b reaches its asymptotic value, this definition should be used because it provides a precise and quantitative basis. Further studies should focus on determining whether such a relation is also valid for defining the positions where quantities such as U_e, k_e, or ε_e reach their asymptotic axial values. The values of the various constants C_U, C_k, C_ε should then be determined in the spirit of the present work. Obviously, complete flow development has not a unique definition, as it strongly depends on the particular physical quantity which is considered.

Another consequence of the previous reasoning is that the variable $(X/D_h)/(U_b D_h/\nu)^{1/4}$ is the one that allows a universal characterization of the development of turbulent flows in ducts, in contrast with the variable $(X/D_h)/(U_b D_h/\nu)$ that is used in the laminar regime (as said in the introduction). The explanation is that characteristic thicknesses (such as δ_1/X) vary like $\mathrm{Re}_x^{-1/2}$ in laminar boundary layers. It should be noticed that for ducts with very large aspect ratio (cf. experiments by Comte-Bellot [13] and by Dean [14]), the entrance length looks clearly smaller, as shown in Fig. 7. In fact, this reveals that full development of the flow is reached when the boundary layer is approximately equal to the half height of the plane channel $d/2$, so that $\delta_1 \approx \delta/8 \approx d/16$ and $\delta_1/D_h \approx 1/32 \approx 0.032$.

In this case, the physical size that should be compared to the thickness of the boundary layer is no more $D_h/2$ (as it is the case for a circular pipe or a square duct), but rather $d/2$, or $D_h/4$. Thus, the above relation (2) cannot be generalized with a universal value of C for any section shape, since L_e should be compared to the real physical size that is bounding the boundary layer development ($d = D_h/2$ for a plane channel for instance), and so the value of the constant C depends on the duct aspect ratio. A systematic study about the impact of the aspect ratio is needed to quantify this trend.

4. Conclusion

The presented results have identified δ_1/D_h as the dimensionless parameter that allows characterizing the acceleration of pipe and duct flows in their development region. The centerline velocity U_e/U_b then appears to evolve as a linear function of this variable δ_1/D_h, with the slope equal to 4. This work also proved that the grouping $(X/D_h)/(U_b D_h/\nu)^{1/4}$ is the one that allows a universal characterization of the development of turbulent flows in ducts, in contrast with $(X/D_h)/(U_b D_h/\nu)$ that is suitable for laminar flows. As a consequence, the entrance length must vary as a function of the power $1/4$ of the global Reynolds number $\mathrm{Re} = U_b D_h/\nu$.

Thus, even though such results had surprisingly never been published before, the development regions of turbulent circular pipes and ducts of square or rectangular cross-sections display very similar behaviour, and this behaviour can be parameterized in a simple universal way in terms of δ_1/D_h. One is therefore inclined to conclude from the present study that, in spite of the presence of secondary vortices which appear in the corners of turbulent ducts, the global properties of the development region of turbulent pipes and ducts are the same and can be quantified through centerline evaluated quantities only.

Further studies will deal with open flumes as well, for which almost no data concern their development region.

Acknowledgement

The authors would like to thank Professor Frank White of the University of Rhode Island for his valuable comments on the work.

References

[1] J. Nikuradse, Turbulent Strömung im Innern des rechteckigen offenen Kanals, VDI-Forschungsheft. 281 (1926) 37–44.
[2] R.G. Deissler, Analytical and experimental investigation of adiabatic turbulent flow in smooth tubes, NACA TN, no. 2138, 1950.
[3] A. Melling, J. Whitelaw, Turbulent flow in rectangular duct, J. Fluid Mech. 78 (1976) 289–315.
[4] F.B. Gessner, J.K. Po, A.F. Emery, Measurements of developing turbulent flow in a square duct, in: F. Durst, B.E. Launder, R. Friedrich, F.W. Schmidt (Eds.), Turbulent Shear Flows 1, Springer-Verlag, Berlin, 1979, pp. 119–136.
[5] A.O. Demuren, W. Rodi, Calculation of turbulence-driven secondary motion in non-circular ducts, J. Fluid Mech. 140 (1984) 189–222.
[6] F. Jaarsma, General design of low speed wind tunnels, Presented at 79th Fluid Dynamics Panel Symposium, Moscow, published in AGARD-CP 585, 1997, pp. 3.1–3.15.
[7] F.M. White, Viscous Fluid Flow, 3rd edition, McGraw–Hill, New York, 2005.
[8] R. Comolet, Mécanique expérimentale des fluides, vol. II, 3rd edition, Masson, Paris, 1982.
[9] F.M. White, Fluid Mechanics, 5th edition, McGraw–Hill, New York, 2003.
[10] H. Schlichting, Boundary Layer Theory, 6th edition, McGraw–Hill, New York, 1968.
[11] B.E. Launder, D.B. Spalding, Lectures in Mathematical Models of Turbulence, Academic Press, London, 1972.
[12] Fluent User's Guide, vol. 3, Tech. rep., Fluent Inc., 2006.
[13] G. Comte-Bellot, Contribution à l'étude de la turbulence de conduite, Thèse de Doctorat d'Etat, Université de Grenoble, 1963.
[14] R.B. Dean, An investigation of shear layer interaction in ducts and diffusers, Ph.D. thesis, University of London, 1974.
[15] M. Coantic, Contribution à l'étude de la structure de la turbulence dans une conduite de section circulaire, Thèse de Doctorat d'Etat, Université d'Aix-Marseille, 1966.
[16] R.B. Dean, Reynolds number dependence of skin friction and other bulk flow variables in two-dimensional rectangular duct flow, J. Fluids Eng. 100 (1978) 215–223.
[17] W. Szablewski, Der Einlauf einer turbulenten Rohrströmung, Ing. Arch. 21 (1953) 323–330.